

CONSTRAINTS ON PHYSICAL CONDITIONS FOR THE ACCELERATION OF ULTRA-HIGH-ENERGY COSMIC RAYS IN NEARBY ACTIVE GALACTIC NUCLEI OBSERVED WITH THE *FERMI* LARGE AREA TELESCOPE

MIKA KAGAYA^{1,2}, HIDEAKI KATAGIRI^{3,4}, TATSUO YOSHIDA³, AND ARISA FUKUDA³

¹Department of General Engineering, National Institute of Technology, Sendai College, 4-16-1 Ayashi-Chuo, Aoba-ku, Sendai-shi, Miyagi 989-3128, Japan

²email: mikagaya@sendai-nct.ac.jp

³College of Science, Ibaraki University, 2-1-1 Bunkyo, Mito-shi, Ibaraki 310-8512, Japan

⁴email: hideaki.katagiri.sci@vc.ibaraki.ac.jp

ABSTRACT

We investigated the possibility of acceleration of ultra-high-energy cosmic rays (UHECRs) in nearby active galactic nuclei (AGNs) using archival multi-wavelength observational data, and then we constrained their physical conditions, i.e., the luminosity of the synchrotron radiation and the size of the acceleration site. First, we investigated the spatial correlation between the arrival directions of UHECRs and the positions of nearby AGNs in the *Fermi* third gamma-ray source catalog. We selected 27 AGNs as candidates of accelerators of UHECRs. Then, we evaluated the physical conditions in the acceleration regions of these AGNs via the Pe’er and Loeb method, which uses the peak luminosity of synchrotron radiation and the peak flux ratio of inverse Compton scattering to synchrotron radiation. From the evaluation, we found that six AGNs have the ability to accelerate ultra-high-energy *protons* in the AGN cores. Furthermore, we found that the minimum acceleration size must be more than a few kpc for acceleration of UHE *protons* in the AGN lobes.

Keywords: ultra high energy cosmic rays — particle acceleration — nearby active galactic nuclei — gamma ray — the *Fermi* Large Area Telescope

1. INTRODUCTION

The origin of ultra-high-energy cosmic rays (UHECRs) ($E > 10^{18}$ eV) is an important astrophysical problem. The acceleration sites and the acceleration mechanisms of UHECRs remain unsolved since their discovery 50-60 years ago (Clark et al. 1961). A part of the UHECRs is thought to be accelerated by nearby active galactic nuclei (AGNs) (e.g., Bierman et al. 1987; Takami et al. 2011). Recently, a spatial correlation between UHECRs and nearby AGNs has been discussed using data observed by cosmic-ray observatories (e.g., Abreu et al. 2010; Abu-Zayyad et al. 2013). However, it is difficult to strongly constrain the origin of UHECRs using spatial correlations because the experimental statistics of UHECRs are insufficient due to the current sensitivity of the cosmic-ray telescopes. Even though several authors have carried out the correlation studies with more detailed statistical methods (e.g., Kashti et al. 2008; Takami et al. 2009), UHECR data with additional statistics are needed to draw a decisive conclusion. To discuss the origin of UHECRs, multi-wavelength observations and spectral energy distributions (SEDs) can be additional important clues. Several authors have discussed the acceleration of UHECRs using multi-wavelength observations (e.g., Murase et al. 2012; Pe’er and Loeb 2012; Zhang et al. 2014). Out of them, Pe’er & Loeb (2012) have derived constraints with regard to the ability of AGNs to produce UHECRs using the peak fluxes due to synchrotron radiation ($(\nu F_\nu)_{\text{peak, sync}}$) and the inverse Compton scattering (IC) ($(\nu F_\nu)_{\text{peak, IC}}$) of high-energy electrons. However, the capacity to accelerate UHECRs has only been discussed for famous high-energy sources such as Centaurus A (Cen A) and M87. In this study, we expand the number of high-energy sources and investigate the possibility of the acceleration of UHECRs in individual AGNs using the Pe’er and Loeb’s method. Gamma-ray observational data in GeV region is required to determine the peak fluxes due to IC ($(\nu F_\nu)_{\text{peak, IC}}$) used in the method. GeV gamma-ray observations have been advanced by recent gamma-ray observations with the *Fermi* Gamma-Ray Space Telescope (Massaro et al. 2016, and references therein). We used gamma-ray data observed by the Large Area Telescope (LAT) onboard the *Fermi* Satellite (Atwood et al. 2009), which operates in a sky-survey observing mode and covers the entire sky every 3h. This satellite has detected

multiple gamma-ray sources, and the third *Fermi*-LAT gamma-ray source catalog (3FGL) includes approximately 1600 AGNs (Acero et al. 2015; Ackermann et al. 2015). In this paper, we evaluated the ability of sources to accelerate UHECRs in nearby AGNs detected by the *Fermi*-LAT, and then we constrained the physical conditions (the luminosity of the synchrotron radiation and the size of the acceleration site) for acceleration of UHECRs.

2. THE SEARCH FOR CANDIDATE SOURCES OF ACCELERATOR OF UHECRS

We selected the candidates for accelerators of UHECRs using the following two steps: (1) We investigated the spatial correlation between UHECRs detected by the Pierre Auger Observatory (Aab et al. 2015) or the Telescope Array (Abbasi et al. 2014) and AGNs in the 3FGL (Acero et al. 2015). We used the observational data from the Telescope Array for the northern hemisphere and the observational data from the Pierre Auger Observatory for the southern hemisphere. The energies of UHECRs observed by the Pierrer Auger observatory and the Telescope Array are over 5.2×10^{19} eV and 5.7×10^{19} eV, respectively. We selected the AGNs including one or more than UHECR within 4° of the positions of AGNs in the 3FGL. The selected radius of 4° is based on the typical uncertainty of an arrival direction of a UHE *proton* due to deflection by the Galactic magnetic field (Takami 2006). If UHECRs are heavy nuclides, the deflection angle due to the Galactic magnetic field is large (e.g., $>50^\circ$ at 5×10^{19} eV Giaconiti et al. (2010)). In this case, we cannot narrow down source candidates of UHECRs. Therefore, in this study, we focused on the acceleration of protons. We found 183 AGNs that have a spatial correlation with UHECRs. (2) We selected AGNs that have redshifts (z) less than 0.1 because the energy loss of UHECRs by pion photoproduction with microwave background photons limits the propagation length to $z \sim 0.1$ (e.g., Greisen 1966; Zatsepin et al. 1976). The redshifts were derived from the NASA/IPAC Extragalactic Database¹ and the Roma BZCAT-5th edition (Massaro et al. 2015). In the end, we identified 27 AGNs as candidates of accelerators of UHECRs (see Table 1).

3. VERIFICATION OF POSSIBILITY OF ACCELERATING UHECRS

First, we briefly explain the theory of Pe'er and Loeb (2012). Assuming that electrons are being accelerated in the same acceleration region of the UHECRs, the energy spectrum due to synchrotron radiation can be obtained at radio, infrared, optical and soft X-ray bands. The peak flux of synchrotron radiation in an AGN can be approximated by Eq. (1),

$$(\nu F_\nu)_{\text{peak, sync}} = \frac{n_e V}{4\pi d_L^2} \left(\frac{4}{3}\right) c \sigma_T \gamma_e^2 \left(\frac{B^2}{8\pi}\right) \mathcal{D}^2. \quad (1)$$

Here, n_e , V , d_L , c , σ_T , γ_e and B are the number density of electrons, the volume of the emission region, the luminosity distance, the light speed, the Thomson cross section, the Lorentz factor of an electron and the strength of the magnetic field, respectively. $\mathcal{D} = [\Gamma(1 - \beta \cos \theta_{\text{ob}})]^{-1}$ is the Doppler factor of a jet for an observing angle θ_{ob} of an AGN, where Γ is the Lorentz factor of the jet and β is the ratio of v to c , where v is the speed of the jet. Here, we assume that we are inside the radiation region of a jet. Therefore, $\theta_{\text{ob}} < \max(\Gamma^{-1}, \theta_{\text{jet}})$ and $\mathcal{D} \simeq \Gamma$, where θ_{jet} is the opening angle of the jet.

The SED of an AGN has a second peak in the high-energy region (hard X-ray and gamma rays) due to IC that results from seed photons. The origin of seed photons can be synchrotron radiation itself (Synchrotron Self-Compton scattering model: SSC model) and/or external radiation fields (External Radiation Compton scattering model: ERC model) originating from the cosmic microwave background (CMB), extragalactic background light (EBL), or dusty torus surrounding an AGN. Here, we do not assume the origin of the seed photons and denote the frequency of a seed photon by ν_{seed} . The frequency of outgoing photons due to IC is $\nu_{\text{IC}} = (4/3)\gamma_e^2 \nu_{\text{in}}$. The peak monochromatic flux of IC is $(F_\nu)_{\text{peak, IC}} = \tau (F_\nu)_{\text{peak, seed}}$, where $\tau \simeq \Delta l n_e \sigma_T$. Here, we approximate the volume of the acceleration region by a cylindrical shape $V = \pi r^2 \Delta l$ with the radius r and the height Δl . Substituting these results into Eq. (1), one obtains

$$(\nu F_\nu)_{\text{peak, sync}} = \frac{1}{4\pi d_L^2} \frac{c B^2 r^2}{8} \mathcal{D}^2 \left(\frac{(\nu F_\nu)_{\text{peak, IC}}}{(\nu F_\nu)_{\text{peak, seed}}} \right). \quad (2)$$

To accelerate particles up to the energy of UHECRs via electromagnetic processes, the particles need to be confined in the acceleration region. Therefore, the size of the acceleration region must be larger than the mean free path of the particles. This condition is given in Eq. (3),

¹ The NASA/IPAC Extragalactic Database (NED) is operated by the Jet Propulsion Laboratory, California Institute of Technology, under contract with the National Aeronautics and Space Administration.

$$r \geq \frac{\eta E_{\text{ob}} \beta}{ZeB}, \quad (3)$$

where r , E_{ob} and Ze are the size of radius of the acceleration region, the observed energy of UHECRs and the charge of UHECRs. η (≥ 1) is the ratio of the mean free path of the particle to the Larmor radius, whose exact value is determined by the details of the particle transportation. Combining Eqs. (2) and (3), we obtain

$$(\nu F_{\nu})_{\text{peak, sync}} \geq \frac{1}{4\pi d_L^2} \frac{c}{8} \left(\frac{\eta E_{\text{ob}}}{Ze} \right)^2 \beta^2 \mathcal{D}^2 \left(\frac{(\nu F_{\nu})_{\text{peak, IC}}}{(\nu F_{\nu})_{\text{peak, seed}}} \right). \quad (4)$$

From Eq. (4), the peak flux due to synchrotron radiation can be constrained using the ratio of the peak fluxes. We evaluated the peak flux due to synchrotron radiation as described in Section 3.1 and 3.2.

Second, we will explain the evaluation method for the peak flux ratio of IC to synchrotron radiation using archival multi-wavelength observational data. The SED data were obtained from the NASA Langley Research Center Atmospheric Science Data Center (ASDC). Each component of the low-energy and the high-energy regions was fitted with a third-order polynomial function using the chi-square method to phenomenologically reproduce the spectrum (Kubo et al. 1998). Figure 1 shows each SED of the AGNs, and the peak flux ratio is summarized in Table 1. Note that the SED of the core of Centaurus A is based on the data of Abdo et al. (2010). Its peak flux ratio was determined by a fitting with the same method. For the SED and the peak ratio of the lobe of Centaurus A, we also used the result of Abdo et al. (2010) because there were insufficient data points in the ASDC.

3.1. CONSTRAINT ON MINIMUM PEAK LUMINOSITY DUE TO SYNCHROTRON RADIATION

In the case that the acceleration region in an AGN is the core, gamma rays from an AGN are typically produced by IC of synchrotron photons by high-energy electrons. Then, the ratio of the peak flux due to IC and synchrotron radiation $Y = (\nu F_{\nu})_{\text{peak, IC}} / (\nu F_{\nu})_{\text{peak, sync}}$ can be used as a probe of the peak luminosity due to synchrotron radiation $L_{\text{peak, sync}}$ in the acceleration site. Here, we have assumed that the seed photons of IC scattering are synchrotron photons (SSC model). In this case, the minimum luminosity is constrained by the ratio of the peak fluxes. From Eq. (4), a constraint on $L_{\text{peak, sync}}$ can be written as

$$L_{\text{peak, sync}} \equiv 4\pi d_L^2 (\nu F_{\nu})_{\text{peak, sync}} \geq \frac{cY}{8} \left(\frac{\eta E_{\text{ob}}}{Ze} \right)^2 \beta^2 \mathcal{D}^2 = 1.0 \times 10^{44} Y \left(\frac{E_{\text{ob}}}{5 \times 10^{19} \text{eV}} \right)^2 \left(\frac{\eta}{Z} \right)^2 \beta^2 \mathcal{D}^2 \text{ erg s}^{-1}. \quad (5)$$

Here, we have assumed $(\eta/Z)\beta\mathcal{D} = 1$ and $Z = 1$. By comparing the minimum constrained value of the luminosity to the observed luminosity, we evaluated the capability of particle acceleration up to the energy of the associated UHECRs. Figure 2 shows the distribution of synchrotron radiation luminosity as a function of Y . The solid line in Figure 2 shows a boundary where an AGN core can accelerate UHECRs of 5×10^{19} eV corresponding to the lowest energy of the observed UHECRs. The dashed line shows a boundary where an AGN core can accelerate the UHECRs up to 8.38×10^{19} eV. This is the maximum of the energies of UHECRs associated with candidate AGNs having the ability to accelerate UHECRs in AGN cores. Moreover, by rearranging Eq. (5) and assuming that $(\eta/Z)\beta\mathcal{D} = 1$, we can obtain the theoretical maximum energies, $E_{\text{max}} = 5 \times 10^{19} (L_{\text{peak, sync}} / 10^{44} \text{ erg s}^{-1})^{1/2} (1/Y)^{1/2}$ eV; they are summarized in Table 1. We found that six AGNs (3FGL J0152.6+0148 (PMN J0152+0146), 3FGL J0353.0-6831 (PKS 0352-686), 3FGL J1444.0-3907 (PKS 1440-389), 3FGL J1517.6-2422 (AP Librae), 3FGL J2009.3-4849 (PKS 2005-489), 3FGL J2202.7+4217 (BL Lacertae)) have the capability of UHECR acceleration in their cores even if UHECRs are composed of UHE *protons*.

Note that the peak flux in the low-energy region of 3FGL J1413.2–6518 (the Circinus galaxy) can be given as an upper limit of the thermal radiation (e.g., IR bump and big blue bump), which is dominant over the synchrotron radiation. The allowable luminosity of the synchrotron radiation can be given as, $L_{\text{peak, sync}} = 6.4 \times 10^{43} (d_L / 1.3 \times 10^{25} \text{ cm})^2 ((\nu F_{\nu})_{\text{peak, IC}} / 2.9 \times 10^{-8} \text{ erg cm}^{-2} \text{ s}^{-1}) (1/Y) \text{ erg s}^{-1}$ ($Y > 0.022$). This locates in the forbidden region in Figure 2. Therefore, we could not strongly constrain the capability of the Circinus galaxy to accelerate of UHECRs.

3.2. CONSTRAINT ON ACCELERATION SIZE OF AGN LOBE

UHECRs can be accelerated in the turbulent outflow or at the termination shock of giant AGN lobes. In this case, the external photons are dominant as seed photons because the energy density of synchrotron photons is negligible (ERC model). When the size of radius of the acceleration region is R_{acc} , the energy density of synchrotron photons is

estimated to be $u'_{\text{sync}} = L_{\text{sync}}/\pi R_{\text{acc}}^2 c \mathcal{D}^3 \simeq 7 \times 10^{-4} (L_{\text{sync}}/10^{44} \text{ erg s}^{-1}) (R_{\text{acc}}/10 \text{ kpc})^{-2} (\mathcal{D}/10)^{-3} \text{ eV cm}^{-3}$ ², which is smaller in comparison with the energy density of CMB, $u'_{\text{CMB}} = u_{\text{CMB}} \Gamma^2 \simeq u_{\text{CMB}} \mathcal{D}^2 = 26 (\mathcal{D}/10)^2 \text{ eV cm}^{-3}$; the primed quantities in the equations indicate measurement in the jet comoving frame (Stawarz et al. 2003). The energy density of EBL (e.g., $u_{\text{EBL}} \simeq 6.5 \times 10^{-3} \text{ eV cm}^{-3}$ (Dole et al. 2006)) has been estimated by several models (e.g., Dominguez et al. 2011; Franceschini et al. 2008; Kneiske et al. 2010), and they have been found to be smaller than the energy density of CMB. Therefore, we used only CMB as seed photons. When CMB photons are dominant as seed photons, the peak flux of the seed photons is calculated by $(\nu F_{\nu})_{\text{peak,seed}} = \pi R_{\text{acc}}^2 c u_{\text{CMB}}/4\pi d_L^2$. Combining the above equation and Eq. (4), we obtain

$$R_{\text{acc}} \geq R_{\text{acc,min}} = \left(\frac{(\nu F_{\nu})_{\text{peak,IC}}}{(\nu F_{\nu})_{\text{peak,sync}}} \right)^{1/2} \left(\frac{1}{8\pi u_{\text{CMB}}} \right)^{1/2} \left(\frac{\eta E_{\text{ob}}}{Z} \right) \beta \mathcal{D} \text{ pc.} \quad (6)$$

Here, we have assumed that $(\eta/Z)\beta\mathcal{D} = 1$. Using Eq. (6), we have calculated the minimum sizes of the acceleration region ($R_{\text{acc,min}}$) required to accelerate the particles up to the energies of the associated UHECRs. Figure 3 shows the distribution of the minimum acceleration sizes of the AGNs; they are summarized in Table 1. We found that the minimum lobe sizes are required to be more than a few kpc in the case that UHECRs are protons.

3.3. ACCELERATION OF UHECRS IN CENTAURUS A

Cen A is the nearest AGN and its apparent size is very large (about 8°). It has frequently been observed in multi-wavelengths (e.g., Steinle et al. 1998; Meisenheimer et al. 2007; Aharonian et al. 2009; Fukazawa et al. 2011). The point-like gamma-ray source and the extended source observed by the *Fermi*-LAT are spatially correlated with the core of Cen A (Abdo et al. 2010) and the giant lobe of Cen A (Abdo et al. 2010), respectively. Moreover, they have the spatial correlation with directions of UHECRs. The peak flux ratio for the core is 3 and its plot is shown as the blue square in Figure 2. Therefore, the core region of Cen A cannot accelerate UHE *protons*, which is consistent with Pe'er and Loeb (2012). In the case of the acceleration of UHECRs in the lobe, we derived the minimum acceleration sizes for the north and the south lobe to be $\geq 105 \text{ kpc}$ and $\geq 138 \text{ kpc}$, respectively. From previous radio observations (e.g., Shain 1958; Burns et al. 1983), the lobe size is $\sim 300 \text{ kpc}$, which is consistent with our estimations of the minimum acceleration sizes.

4. DISCUSSION AND CONCLUSION

We evaluated whether the selected AGNs could accelerate UHE *protons* using the peak synchrotron luminosity and the ratio of the peak fluxes. We found that 27 candidate sources for accelerators of UHECRs from the selection using the spatial correlation between the directions of UHECRs and the positions of the AGNs in the 3FGL catalog. From the constraints imposed by the peak flux ratios, we found that the UHE *protons* can be accelerated in six AGNs cores. All these sources have been classified as BL Lacertae objects. We note that it does not rule out the possibility that the UHECRs in the six AGNs could be accelerated in other regions such as AGN lobes. Here, we calculated the probability that all of the selected six AGNs were BL Lacertae objects coincidentally. Out of blazars whose redshifts are < 0.1 , the sources are 69.5% BL Lacertae object, 3.4% flat-spectrum radio quasar (FSRQ), and 27.1% blazar candidate of uncertainty type (BCU). The classification of the BCU sources was estimated using an artificial neural network method to quantify the likelihood of each 3FGL BCU being more similar to a BL Lacertae or a FSRQ (Chiaro et al. 2016). Using this classification, the percentage changed to 91.5% BL Lacertae, 3.4 % FSRQ, and 5.1% remaining BCUs. The probability that all six sources are BL Lacertae objects was estimated to be 58.7%. Therefore, we cannot rule out the possibility of the chance coincidence. Note that the core regions of f AGNs cannot be acceleration sites of UHE *protons*; however, the possibility of accelerating UHECRs in these sources cannot be ruled out in the case that UHECRs are composed of heavy nuclei, and the composition of UHECRs is still debated (e.g., Abbasi et al. 2015; Cazon et al. 2012; Abbasi et al. 2010).

Assuming that UHECRs are accelerated in the AGN lobes, we found that the minimum sizes of acceleration regions of the candidate sources are required to be more than a few kpc. Out of the 27 sources in Table 1, the physical sizes of the radio galaxies are known due to previous radio and optical observations. In this paper, four radio galaxies (3FGL J0418.5+3813c (3C 111), 3FGL J1145.1+1953 (3C 264), 3FGL J1324.0–4330e (Centaurus A) and 3FGL J1346.6–6027 (Centaurus B)) were selected as candidate sources. Each minimum acceleration size estimated in this paper and each

² We note that the Doppler beaming factor, \mathcal{D} , depends on the observing angle θ_{ob} . When an observer is inside the radiation region of the jet, $\mathcal{D} \simeq \Gamma$ because θ_{ob} is smaller than the opening angle of the jet. Conversely, if θ_{ob} is large (e.g., 90°), then $\mathcal{D} \simeq 1/\Gamma$. The energy density of the latter case might become larger than that of the former case. However, because gamma-ray emitting AGNs typically have small observing angles, we infer that the above assumptions for estimating the energy density are reasonable.

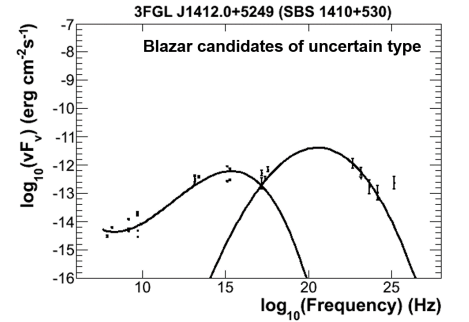
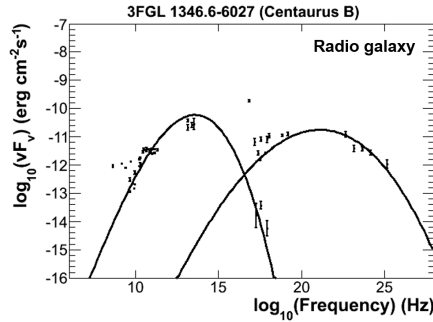
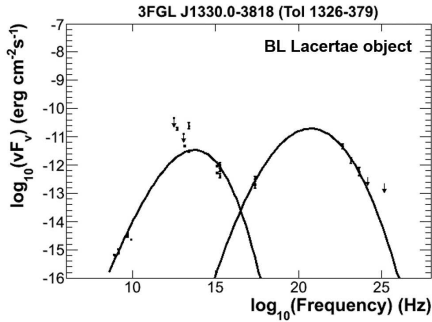
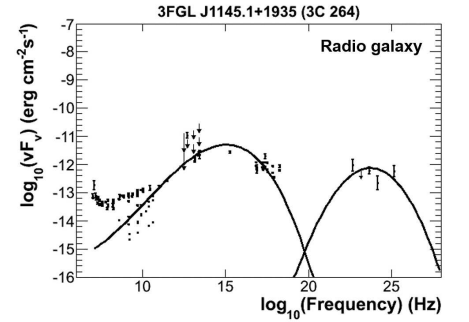
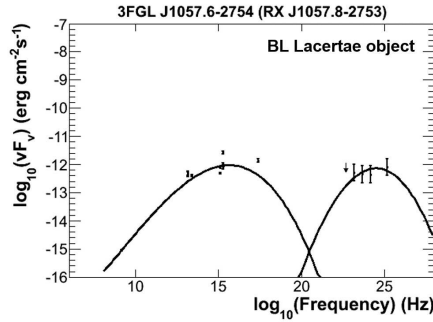
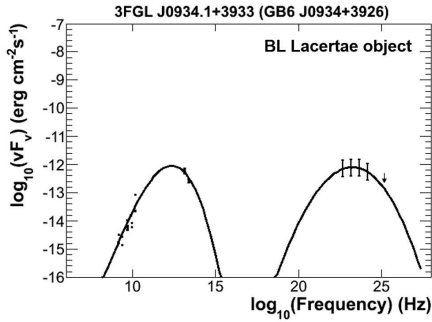
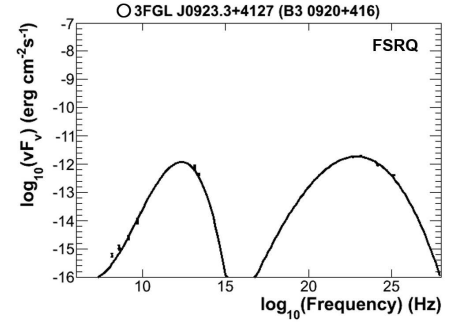
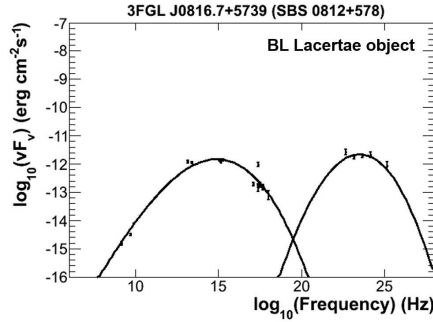
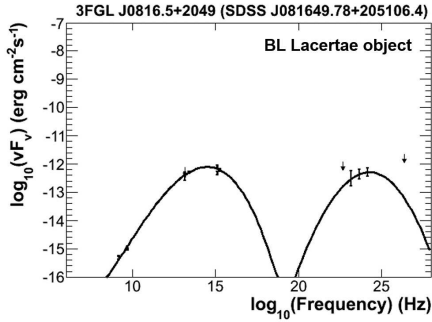
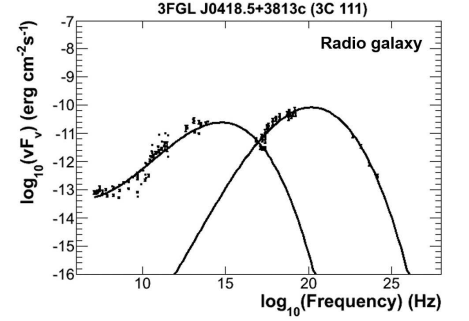
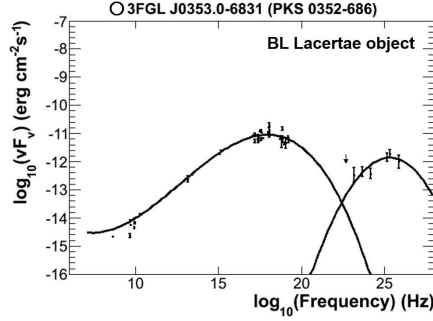
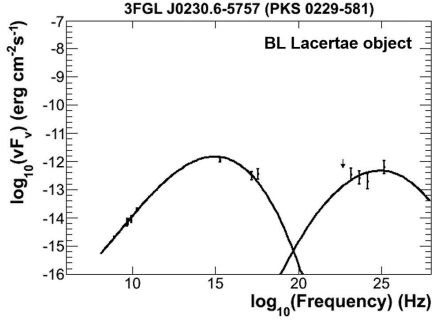
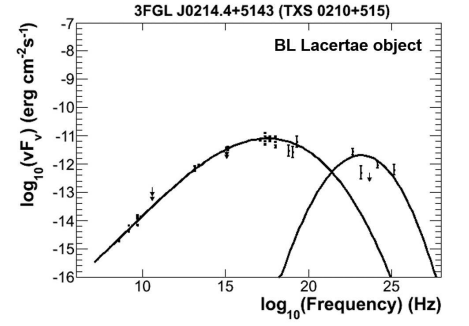
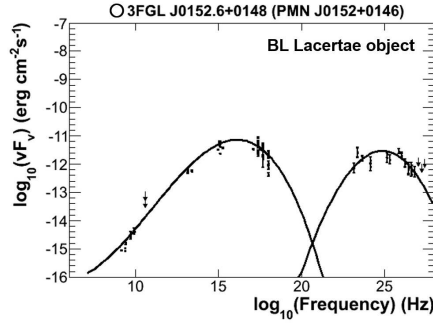
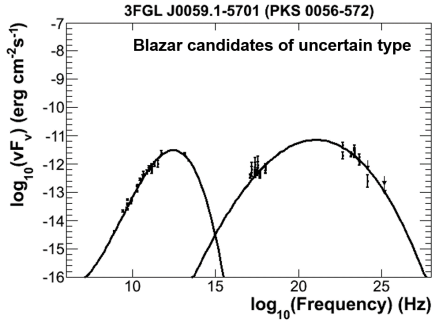
real lobe size are summarized in Table 2. We confirmed that the real physical sizes of these radio galaxies are larger than the estimated sizes of acceleration regions. This is consistent with the hypothesis that these radio galaxies accelerate UHECRs in their lobes (e.g., Baum et al. 1988; Black et al. 1997; Jones et al. 2001; Abdo et al. 2010).

We found 183 AGNs that have the spatial correlation between the directions of UHECRs and the positions in the 3FGL catalog; however, their redshifts of 69 out of 183 are unknown. If their redshifts can be obtained in future observations, we can systematically evaluate the possibility of acceleration of UHECRs in these AGNs. In addition, we found 120 unidentified gamma-ray sources that are spatially correlated with UHECRs. These sources could significantly contribute to the acceleration of UHECRs. We plan to observe these sources with optical telescopes for the determination of their redshifts and source types. If the sources are AGNs with $z < 0.1$, we can discuss whether they can accelerate UHECRs using the evaluation method established in this paper. Several sources have already been observed by the SOAR 4 m optical telescope (Alvarez Crespo et al. 2015).

This study was supported by Grant-in-Aid for JSPS Fellows No. 259495. Special thanks to Dr. Hajime Takami and Prof. Tokonatsu Yamamoto. We would also like to thank the anonymous referees for a careful reading of the manuscript and very helpful comments.

REFERENCES

- Aab, A., Abreu, P., Aglietta, M., et al. 2015, *ApJ*, 804, 15
 Abbasi, R. U., Abu-Zayyad, T., Allen, M., et al. 2015, *APh*, 64, 49
 Abbasi, R. U., Abe, M., Abu-Zayyad, T., et al. 2014, *The Astrophysical Journal Letters*, 790, 49
 Abbasi, R. U., Abu-Zayyad, T., Ak-Seady, M., et al. 2010, *PhRvL*, 104, 161101
 Abdo, A. A., Ackermann, M., Ajello, M., et al. 2010, *ApJ*, 719, 1433
 Abdo, A. A., Ackermann, M., Ajello, M., et al. 2010, *Sci*, 328, 725
 Abreu, P., Aglietta, M., Ahn, E. J., et al. 2010, *APh*, 34, 314
 Abu-Zayyad, T., Aida, R., Allen, M., et al. 2013, *ApJ*, 777, 88
 Acero, F., Ackermann, M., Ajello, M., et al. (The *Fermi* LAT Collaboration) 2015, *ApJ*, 218, 23
 Ackermann, M., Ajello, M., Atwood, W. B., et al. 2015, *ApJ*, 810, 14
 Aharonian, F., Akhperjanian, A. G., Anton, G., et al. 2009, *ApJ*, 695, L40
 Alvarez Crespo, N., Massaro, F., Milisavljevic, D., et al. 2015, *AJ*, 151, 163
 Atwood, W. B., Abdo, A. A., Ackermann, M., et al. (The *Fermi* LAT Collaboration) 2009, *ApJ*, 697, 1071
 Biermann, P. L., & Strittmatter, P. A., 1987, *ApJ*, 322, 643
 Black, A. R. S., Baum, S. A., Leahy, J. P., et al. 1997, *MNRAS*, 256, 186
 Baum, S. A., Heckman, T. M., Bridge, A., et al. 1988 *ApJS*, 68, 643
 Burns, J. O., Feigelson, E. D., Schreier, E. J., 1983, *ApJ*, 273, 128
 Cazon, L., & the Pierre Auger Collaboration, 2012, *JPCS*, 375, 052003
 Chiaro, G., Salvetti, D., La Mura, G., et al. 2016, *MNRAS*, 462, 3180
 Clark, G., Earl, J., Kraushaar, W., et al. 1961, *PhRv*, 122, 637
 Dole, H., Lagache, G., Puget, J.-L., et al. 2006, *A&A*, 451, 417
 Dominguez, A., Primack, J. R., & Rosario, D. J., 2011, *MNRAS*, 410, 2556
 Franceschini, A., Rodighiero, G., & Vaccari, M., 2008, *A&A*, 487, 837
 Fukazawa, Y., Hiragi, K., Yamazaki, S., et al. 2011, *ApJ*, 743, 124
 Giacinti, G., KachelrieB, M., Semikoz, D. V., & Sigl, G., 2010, *JCAP*, 8, 36
 Greisen, K., 1966, *Physical Review Letters*, 16, 748
 Hardcastle, M. J., Cheung, C. C., Feain, I. J., & Stawarz, L., 2009, *MNRAS*, 393, 1041
 Jones, P. A., Lloyd, B. D., McAdam, W. B., et al. 2001, *MNRAS*, 325, 817
 Junkes, N., Haynes, R. F., Harnett, J. I., et al. 1993, *A&A*, 269, 29
 Kashti, T., & Waxman, E., 2008, *JCAP*, 5, 6
 Kneiske, T. M., & Dole, H., 2010, *A&A*, 515, A19
 Kubo, H., Takahashi, T., Madejski, G., et al. 1998, *ApJ*, 504, 693
 Massaro, F., Thompson, D. J., & Ferrara, E. C., 2016, *A&A Rv*, 24, 2
 Massaro, E., Maselli, A., Leto, C., et al. 2015, *AP&SS*, 357, 75
 Meisenheimer, K., Tristram, K. R. W., Jaffe, W., et al. 2007, *A&A*, 471, 453
 Murase, K., Dermer, C. D., Takami, H., et al. 2012, *ApJ*, 749, 63
 Pe'er, A., & Loeb, A., 2012, *JCAP*, 3, 7
 Shain, C. A., 1958, *AuJPh.*, 11, 517
 Stawarz, L., Sikora, M., & Ostrowski, M., 2003, *ApJ*, 597, 186
 Steinle, H., Bennett, K., Bloemen, H., et al. 1998, *A&A*, 330, 97
 Takami, H., 2006, *ApJ*, 639, 803
 Takami, H., Nishimichi, T., Yahata, K., et al. 2009, *JCAP*, 6, 31
 Takami, H., & Horiuchi, S., 2011, *APh*, 34, 749
 Zatsepin, G. T., & Kuzumin, V. A., 1976, *JETPL*, 4, 78
 Zhang, B., Zhao, X., Cao, Z., et al. 2014, *IJAA*, 4, 499



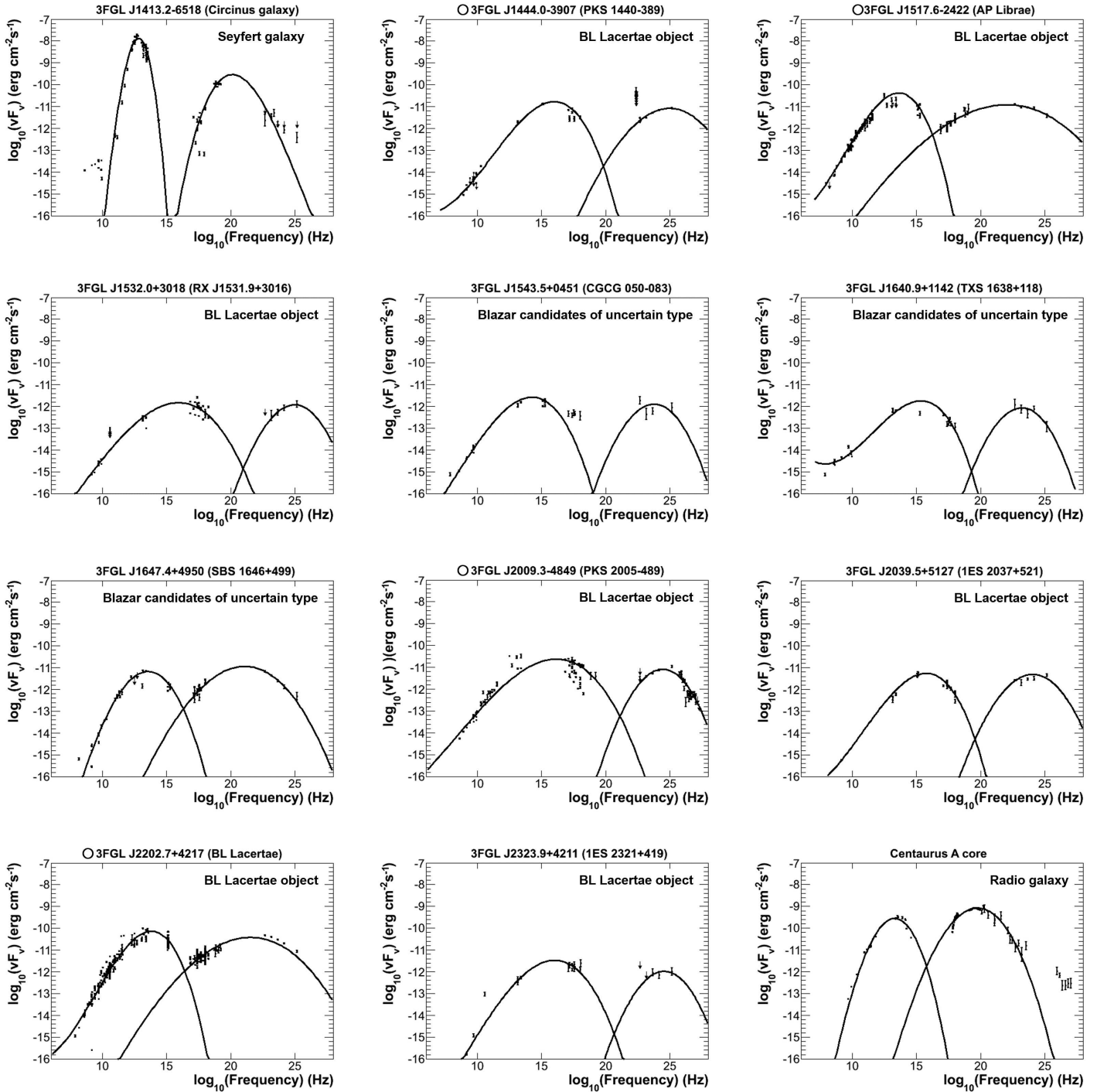


Figure 1. SEDs of 27 AGNs, which are the candidates of accelerators of UHECR. The SED data were obtained from the NASA Langley Research Center Atmospheric Science Data Center (ASDC). The lines are the results of fitting the observational data. The lines at the low-energy region and the high-energy region show the energy peak fluxes due to synchrotron radiation and IC, respectively. The circle marks beside the source names denote that the AGNs have the capability of UHECR acceleration in their cores.

Table 1. Characteristics of the candidate sources of accelerators of UHECRs

3FGL source	Associated source name	R.A. (J2000)	decl. (J2000)	Type	redshift	E_{ob} (EeV)	E_{max} (EeV)	Y	$L_{\text{sync,peak,ob}}$ (erg s^{-1})	$L_{\text{sync,peak,const}}$ (erg s^{-1})	core acceleration	R_{acc} (kpc)
J0059.1–5701	PKS 0056–572	14.796	–57.022	BCU	0.018	57.3	5.0	2.285	2.28×10^{42}	3.00×10^{44}	no	30
J0152.6+0148	PMN J0152+0146	28.162	1.808	BLL	0.080	83.8	85.2	0.400	1.16×10^{44}	1.12×10^{44}	yes	19
J0214.4+5413	TXS 0210+515	33.611	51.723	BLL	0.049	78.7	67.1	0.254	4.58×10^{43}	6.29×10^{43}	no	14
J0230.6–5757	PKS 0229–581	37.671	–57.957	BLL	0.032	62.6, 54.3	16.7	0.317	3.53×10^{42}	4.96×10^{43}	no	12
J0353.0–6831	PKS 0352–686	58.273	–68.517	BLL	0.087	68.8	167.0	0.154	1.72×10^{44}	2.91×10^{43}	yes	9
J0418.5+3813c	3C 111	64.640	38.221	RDG	0.049	68.2	31.4	3.432	1.35×10^{44}	6.39×10^{44}	no	44
J0816.5+2049	SDSS J081649.78+205106.4	124.144	20.811	BLL	0.058	60.3	15.6	0.651	6.31×10^{42}	9.46×10^{43}	no	17
J0816.7+5739	SBS 0812+578	124.183	57.660	BLL	0.054	75.0	13.2	1.478	1.03×10^{43}	3.33×10^{44}	no	32
J0923.3+4127	B3 0920+416	140.846	41.463	FSRQ	0.028	92.3, 68.9	5.8	1.584	2.14×10^{42}	5.40×10^{44}	no	41
J0934.1+3933	GB6 J0934+3926	143.549	39.564	BLL	0.044	92.2	10.7	0.890	4.11×10^{42}	3.03×10^{44}	no	31
J1057.6–2754	RX J1057.8–2753	64.640	38.221	BLL	0.090	84.8	24.7	0.783	1.91×10^{43}	2.25×10^{44}	no	26
J1145.1+1935	3C 264	176.287	19.594	RDG	0.022	68.8	30.6	0.148	5.54×10^{42}	2.81×10^{43}	no	9
J1324.0–4330e	Centaurus A lobe (north)	201.000	–43.500	RDG	0.018	60.0	-	25	-	-	-	105
J1324.0–4330e	Centaurus A lobe (south)	201.000	–43.500	RDG	0.018	60.0	-	43	-	-	-	138
J1325.4–4301	Centaurus A core	201.367	–43.031	RDG	0.018	60.0	42.1	2.986	2.11×10^{44}	4.30×10^{44}	no	-
J1330.0–3818	Tol 1326–379	202.506	–38.313	BLL	0.028	53.3	5.2	5.753	6.10×10^{42}	6.54×10^{44}	no	45
J1346.6–6027	Centaurus B	206.652	–60.454	RDG	0.013	66.7	43.2	0.298	2.23×10^{43}	5.30×10^{43}	no	13
J1412.0+5249	SBS 1410+530	213.02	52.817	BCU	0.076	69.2	5.64	6.786	8.63×10^{43}	1.30×10^{45}	no	63
J1413.2–6518	Circinus galaxy	213.317	–65.304	SEY	0.001	64.8	-	-	-	-	-	-
J1444.0–3907	PKS 1440–389	221.009	–39.130	BLL	0.065	58.8	92.4	0.500	1.71×10^{44}	6.92×10^{43}	yes	15
J1517.6–2422	AP Librae	229.421	–24.376	BLL	0.049	69.6	143	0.290	2.38×10^{44}	5.62×10^{43}	yes	13
J1532.0+3018	RX J1531.9+3016	233.022	30.308	BLL	0.064	62.5	21.3	0.804	1.46×10^{43}	1.26×10^{44}	no	20
J1543.5+0451	CGCG 050–083	235.879	4.864	BCU	0.039	69.6	22.7	0.480	9.90×10^{42}	9.31×10^{43}	no	17
J1640.9+1142	TXS 1638+118	250.247	11.707	BCU	0.078	56.2	37.7	0.477	2.71×10^{43}	6.02×10^{43}	no	14
J1647.4+4950	SBS 1646+499	251.873	49.837	BCU	0.048	57.6	22.9	1.733	3.63×10^{43}	2.30×10^{44}	no	27
J2009.3–4849	PKS 2005–489	302.349	–48.828	BLL	0.071	54.4	199	0.251	4.00×10^{44}	2.98×10^{43}	yes	10
J2039.5+5217	1ES 2037+521	309.894	52.298	BLL	0.053	57.3, 57.9	32.1	0.894	3.69×10^{43}	1.20×10^{44}	no	19
J2202.7+4217	BL Lacertae	330.687	42.284	BLL	0.069	53.5, 56.8	202	0.521	8.49×10^{44}	6.72×10^{43}	yes	14
J2323.9+4211	1ES 2321+419	350.981	42.184	BLL	0.059	122	47.5	0.311	2.81×10^{43}	1.86×10^{44}	no	24

Note; Columns 1 and 2 are the 3FGL and the associated source name, respectively. Columns 3 and 4 are the J2000 coordinates of the 3FGL sources. Column 5 denotes the types of the gamma-ray sources; BLL, FSRQ, RDG, SEY, and BCU indicate BL Lacertae objects, flat-spectrum radio quasars, radio galaxies, Seyfert galaxies, and blazar candidates of uncertain type, respectively. Column 6 is the redshift. Column 7 is the energy of UHECR that has a spatial correlation with the 3FGL sources; column 8 is the maximum energy of UHECRs estimated using the ratio of the peak fluxes Y . Here, for the SED and Y of the lobe of Centaurus A, we used the result from Abdo et al. (2010) because there were insufficient data points in the ASDC. Columns 10 and 11 denote the observed peak luminosity due to synchrotron radiation and constrained peak luminosity at low energy, respectively. Column 12 denotes the results of the evaluation of the capability of UHECR acceleration in the AGN cores. Column 13 is the minimum size of the acceleration regions of the candidate AGNs.

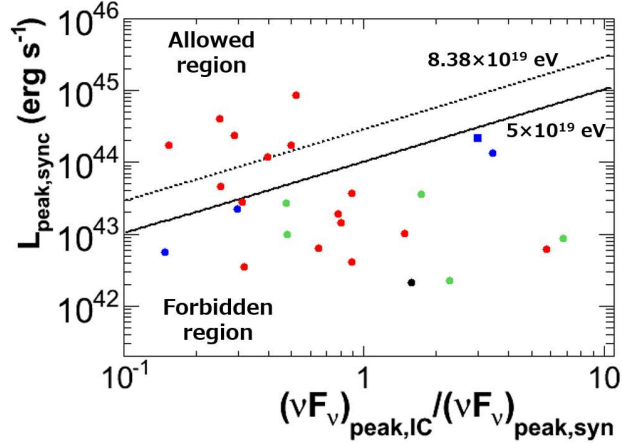


Figure 2. Distribution of minimum peak luminosities of synchrotron radiation in candidate sources as a function of $Y = (\nu F_\nu)_{\text{peak,IC}} / (\nu F_\nu)_{\text{peak,sync}}$. Assuming SSC model, we constrained the capability of UHECR acceleration in AGN cores. $(\eta E_{\text{ob}}/Z)\beta\mathcal{D} = 1$ and $Z = 1$ for proton. The red dots, blue ones, green ones and black ones show BL Lacertae sources, radio galaxies, blazar candidates of uncertain type and FSRQs, respectively. The blue square denotes Centaurus A. The solid line shows a boundary where an AGN core can accelerate the UHECRs of 5×10^{19} eV corresponding to the lowest energy of observed UHECRs. The dashed line shows a boundary where the AGN core can accelerate the UHECRs up to 8.38×10^{19} eV. This is the maximum of the energies of UHECRs associated with the candidate AGNs that have the ability of UHECR acceleration in AGN cores. We note that 3FGL J1413.2–6518 (the Circinus galaxy) was excluded because the peak flux in the low-energy region of its SED can be given as an upper limit due to the thermal radiation, then the peak luminosity of its synchrotron radiation locates in the forbidden region (see section 3.1).

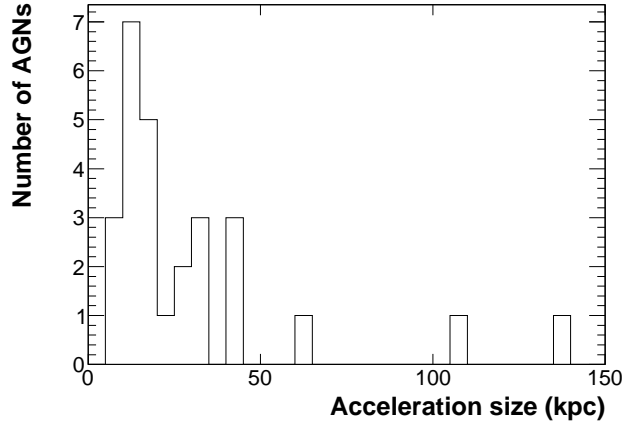


Figure 3. Distribution of the minimum sizes of the acceleration regions of the candidate AGNs to accelerate UHECRs up to the energies of the associated UHECRs.

Table 2. Comparison of lobe sizes of radio galaxies

3FGL Source	Associated Source Name	Type	$R_{\text{acc,min}}$ (kpc)	Lobe Size (kpc)	Reference
J0418.5+3813c	3C 111	FR II	44	355	Black et al. (1997)
J1145.1+1935	3C 264	FR I	9	140	Baum et al. (1988)
J1324.0–4330e	Centaurus A lobe (north)	FR I	105	300	Abdo et al. (2010)
J1324.0–4330e	Centaurus A lobe (south)	FR I	138	300	Abdo et al. (2010)
J1346.6–6027	Centaurus B	FR II	13	130	Jones et al. (2001)

Note. – Column 1 and 2 are the 3FGL source name and the associated source name, column 3 is the types of radio galaxies, column 4 and 5 are the minimum size of the acceleration regions required for UHECR acceleration and the real lobe sizes observed by the radio observations, and column 6 is the reference.